Flow in Severe Thunderstorms Observed by Dual-Doppler Radar

EDWARD A. BRANDES

National Severe Storms Laboratory, NOAA, Norman, Okla. 73069

(Manuscript received 4 June 1976, in revised form 20 October 1976)

ABSTRACT

Dual-Doppler (S-band) radar observations are used to describe both the three-dimensional flow and a life cycle of a severe thunderstorm on 6 June 1974. The primary updraft region was near a small mesocyclonic circulation located on the storm's right (southern) flank. Rotation was first noted aloft (between 3 and 5 km elevation) and lowered with time. During the mature stage, major downdrafts were found on the storm's western edge and within the left forward (northeastern) quadrant. Outflow from both downdrafts combined near the cloud base to form a vigorous gust front. Hook echo formation is attributed to horizontal acceleration of low-level droplet-laden air as the downdrafts intensified and the outflow interacted with the inward-spiraling updraft.

1. Introduction

Recent investigations by Lhermitte and Gilet (1975), Ray *et al.* (1975) and Kropfli and Miller (1976) demonstrate that Doppler radar is a powerful sensor for kinematic studies of precipitating weather systems. Among the important applications is not only the detection of severe convective storms but also the determination of their three-dimensional flow structure and evolution.

On 6 June 1974 a short line of severe thunderstorms developed in central Oklahoma along a slow-moving cold front. Following formation these storms moved ahead of the front, into the National Severe Storms Laboratory (NSSL) dual-Doppler area, through a surface observation mesonetwork and across a dense raingage network. This paper primarily addresses the three-dimensional flow structure and life cycle of one storm which possessed severe right moving characteristics (Browning, 1964; Marwitz, 1972).

2. Dual-Doppler radar observations and analysis

The available dual-Doppler radar data consisted of three coordinated volumetric sampling sequences with measurements at 1° azimuthal, 1° or 2° elevation and 0.6 km range intervals. Some characteristics of the two radars are given in Table 1. Details concerning data acquisition and signal processing techniques can be found in Ray *et al.* (1975) and Sirmans and Bumgarner (1975).

Radial velocity and reflectivity (Z) measurements from each radar were projected to common horizontal planes (2×2 km grid spacing) with an exponential weighting function (Barnes, 1964) having an oblate spheriod influence region (horizontal and vertical radii of 3 and 2 km, respectively). Observation weights varied from 1.0 for radar measurements coincident with gridpoint locations to 0.03 for measurements at the periphery of the influence region. Interpolated data planes with 1 km vertical separation began at 0.3 km AGL (average radar beam height at 0° antenna elevation).[1]

Only observations with radar reflectivities $\geqslant 20$ dBZ were considered and all observations were adjusted for mean storm motion to a common reference time near the midpoint of data collection. It is assumed that storm structure remained fixed during the sampling period (approximately 5 min).

Cartesian wind components were determined with a modified version of the analysis scheme proposed by Armijo (1969). In brief, radial velocity measurements (V_R) at the same point in space (x,y,z) are related to Cartesian wind components by

$$V_{R1}=[x_1u+y_1v+z(w+V_t)]/R_1, \quad (1)$$

$$V_{R2}=[x_2u+y_2v+z(w+V_t)]/R_2. \quad (2)$$

The wind components $u(x,y,z)$, $v(x,y,z)$ and $w(x,y,z)$ are in the x (east), y (north) and z (vertical) directions, respectively; the slant range $R=(x^2+y^2+z^2)^{\frac{1}{2}}$; and $V_t(x,y,z)$ is the hydrometeor terminal velocity (estimated from radar reflectivity measurements). The numerical subscripts are used to distinguish the two radars; the origin is at the Norman radar (number 1).

Eqs. (1) and (2) are solved for u and v and expressed as

$$u=Aw+B, \quad (3)$$

$$v=Cw+D. \quad (4)$$

A and C are functions of the distances x_1, y_1, x_2, y_2 and z; while B and D also include the terms V_{R1}, V_{R2} and

[1] For MSL add 0.37 km.

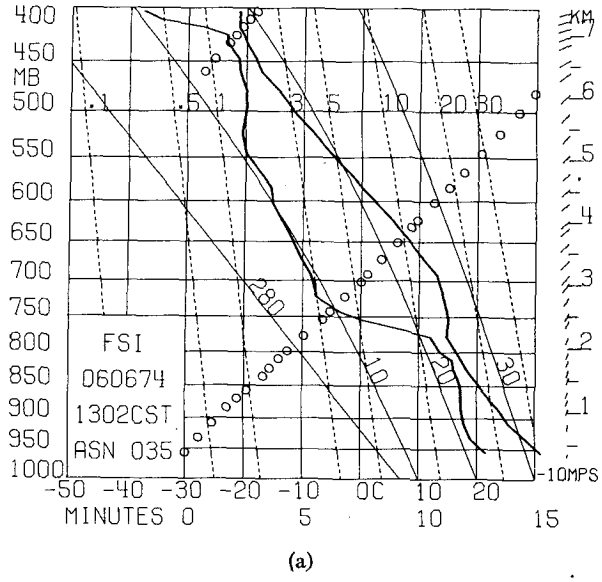

(a)

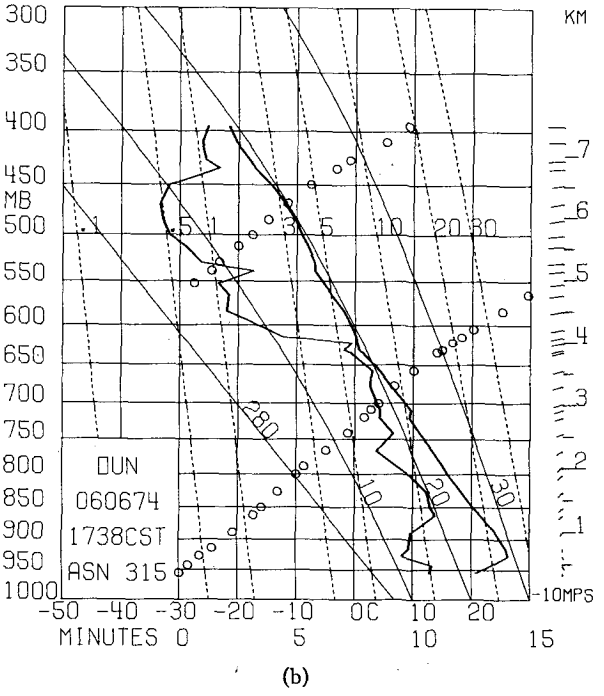

(b)

FIG. 1. Stüve diagrams for (a) Fort Sill (1302 CST) and (b) Norman, Okla. (1738 CST). Wind scale is at lower right and balloon ascent (MSL height versus time) shown by a series of circles.

V_t. To complete the set of equations an anelastic equation of continuity (Ogura and Phillips, 1962)

$$\frac{\partial w}{\partial z}=-\left(\frac{\partial u}{\partial x}+\frac{\partial v}{\partial y}\right)+kw \qquad (5)$$

is used, where $k=-[\partial(\ln\rho)/\partial z]$ is taken from an appropriate sounding.

Calculations of w are produced by finite-difference technique using (5) and involves iterations with (3) and (4). Lower boundary (ground) conditions require $w(x,y,z_0)=0$ and assumes the average divergence below 0.3 km (average 0° radar beam height) is a fraction of that calculated at 0.3 km from the dominant measured terms B and D of (3) and (4). Fine directional agreement and small speed differences found between zero elevation Doppler measurements and observed mesonetwork winds indicated the mean divergence between ground and 0.3 km was slightly less than that calculated at 0.3 km (about 90%). Rogers' (1964) formula (i.e., $V_t=-3.8Z^{1/14}$), combined with the Foote and du Toit (1969) density-height correction, provided an adjustment for precipitation particle (assumed liquid) terminal velocity. Uncertainty arises, primarily in w, due to errors in the determination of derivatives in (5).

Within this study, analyzed products included the horizontal perturbation wind (level mean removed), vertical wind, horizontal divergence and vertical component of vorticity. It is worth noting that except near the ground, mean winds removed from each analysis level (Section 4) approximated environmental rawinsonde observations (Fig. 1).

3. Thunderstorm environment

Environmental wind, temperature and moisture profiles given in Fig. 1a are representative of conditions ahead of the thundershowers. The atmosphere was conditionally unstable; there was a surface-based moisture layer nearly 2 km deep that was capped by very dry air (lifted index, −9°C). A rawinsonde released behind the squall line and east of the cold

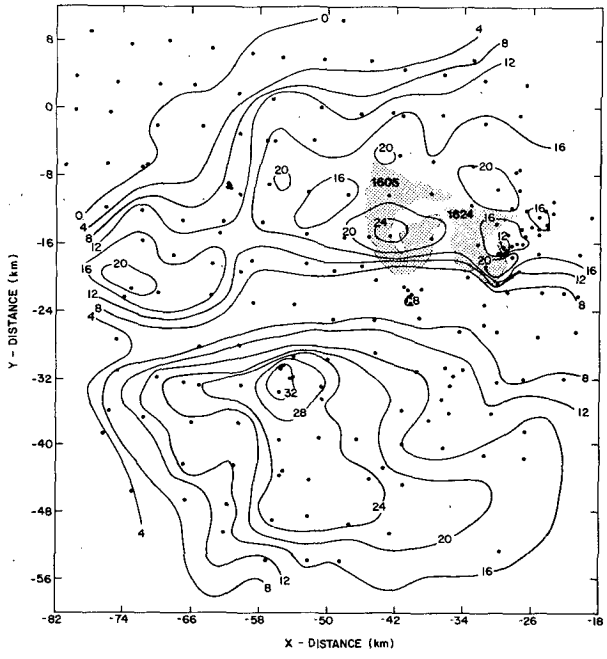

FIG. 2. Squall line total rainfall deposition (mm) within dense raingage network. Contours have been drawn with the aid of an objective analysis routine that combines gage and radar observations (Brandes, 1975).

TABLE 1. Doppler radar characteristics.

	Norman radar	Cimarron radar*
Peak transmitted power (W)	$7.5\times(10^5)$	$5.0\times(10^5)$
Pulse length (m)	150	150
Pulse repetition time (μs)	768	768
Wavelength (cm)	10.52	10.94
Circular beam width (deg)	0.8	0.8
Unambiguous velocity interval (m s^{-1})	34.2	35.6
Unambiguous range (km)	115	115
Antenna gain (dB)	46.8	46.8

* The Cimarron Field facility is approximately 40 km northwest of Norman, Okla.

front (Fig. 1b) revealed substantial modification by convection below 600 mb. Convergence in the region of squall line formation is indicated by the approximate 30° clockwise wind-direction shift between ambient flow east and west of the thunderstorms. Reported cumulus cloud bases were 1.4 km and the mean wind in the cloud bearing layer was 245° at 20 m s^{-1}.

4. Storm structure and life cycle

The severe right-moving storm was sampled simultaneously by the two radars at times which correspond roughly to formation, mature stage and beginnings of decline. Between dual-Doppler data collections, evolution was monitored with single Doppler observations (real time velocity and reflectivity displays) from the Norman radar and with reflectivity observations from NSSL's WSR-57 surveillance radar. Storm total rainfall deposition within a dense raingage network from the severe right-moving storm and other neighboring storms in the squall line is presented in Fig. 2.

a. Early storm development: 1525 CST[2]

The main storm of interest formed when the northeastward moving and developing cell (labeled B in Fig. 3a) merged with the western portion of the east-northeastward moving storm cell A. Rainfall deposition (Fig. 2) increased abruptly as the sections combined. Storm B was the first and largest of several cells that merged with the southern flank of A. These smaller cells were similar to the "feeder clouds" described by Dennis *et al.* (1970) and added a propagative component to the motion of the combined storm AB (from 280° at 12.5 m s^{-1}). Movement across the low-level moisture field is an additional factor which may account for the persistent large storm size (see Fankhauser, 1971).

Fig. 3 shows the general convergence and cyclonic shear between air entering forward and rear quadrants of individual storms in the squall line. Low-level flow (Fig. 3a) converged between A and B (maximum convergence 0.2×10^{-2} s^{-1} on the 2 km grid) and possessed positive vorticity (peak value: 0.2×10^{-2} s^{-1}). At 3.3 and 4.3 km elevation (see Figs. 3c and 3d), a closed cyclonic circulation was detectable near the updraft maximum on the southern flank of A. Located in the northwestern quadrant of A and western portions of B, concurrent updraft maxima were nonrotating and the source air beneath these updrafts showed near zero net vorticity.

Storms farther south (C and D, Fig. 3a) produced large hail along the paths of their principal updrafts (see Table 2). Time uncertainties in the hail reports and infrequent dual-Doppler sampling precludes a more comprehensive correlation. "Noise" present in the wind patterns of these storms may be due to the small acute angle between radial velocity measurements of the two radars and the coarse azimuthal data spacing at these distances. A weak cyclonic circulation near the main updraft of storm C contained mostly downdrafts aloft (Fig. 3d). At 8.3 km elevation (not shown), circulation was scarcely perceptible and the flow was strongly divergent. Storm C produced the small rainfall maximum in the western part of the raingage network (Fig. 2) and dissipated rapidly after 1530 (all times CST). Small-scale remnants (reflectivity cores), moving with the mean environmental wind, merged with the combined storm AB.

Light rainfall accumulations in the southwestern portion of the gage network suggest D was in the developing stage at 1525. During its lifetime, this storm did not exhibit strong rotational characteristics, but while dissipating (after 1600) merged with yet another storm farther south that later produced a mesocyclone.

b. Mature stage: 1616 CST

At 1616, dual-Doppler measurements revealed wind flow about the axis of rotation (Storm AB) had intensified, the circulation (vortex) had lowered below cloud

TABLE 2. Reports of large hail ($\geq$1.3 cm) and related severe weather phenomena from volunteer observer network including time (CST) of occurrence and maximum hail diameter (cm) for 6 June 1974. Times and sizes are approximate.

Locations plotted on Fig. 3a (1525 CST)			
(1)	1510	3.7	
(2)	1531	1.3	
(3)	1530	3.7	
(4)	1515	2.5	
(5)	1510	2.5	
(6)	1525	6.4	
Locations plotted on Fig. 4a (1616 CST)			
(1)	1545	1.3	Wind damage
(2)	Unknown	1.9	Wind damage
(3)	1620	1.3	Wind damage

[2] Differences, primarily in vertical velocity, may be noted from a simple incompressible analysis presented at the *Ninth Conference on Severe Local Storms*, 21–23 October 1975, Norman, Okla.

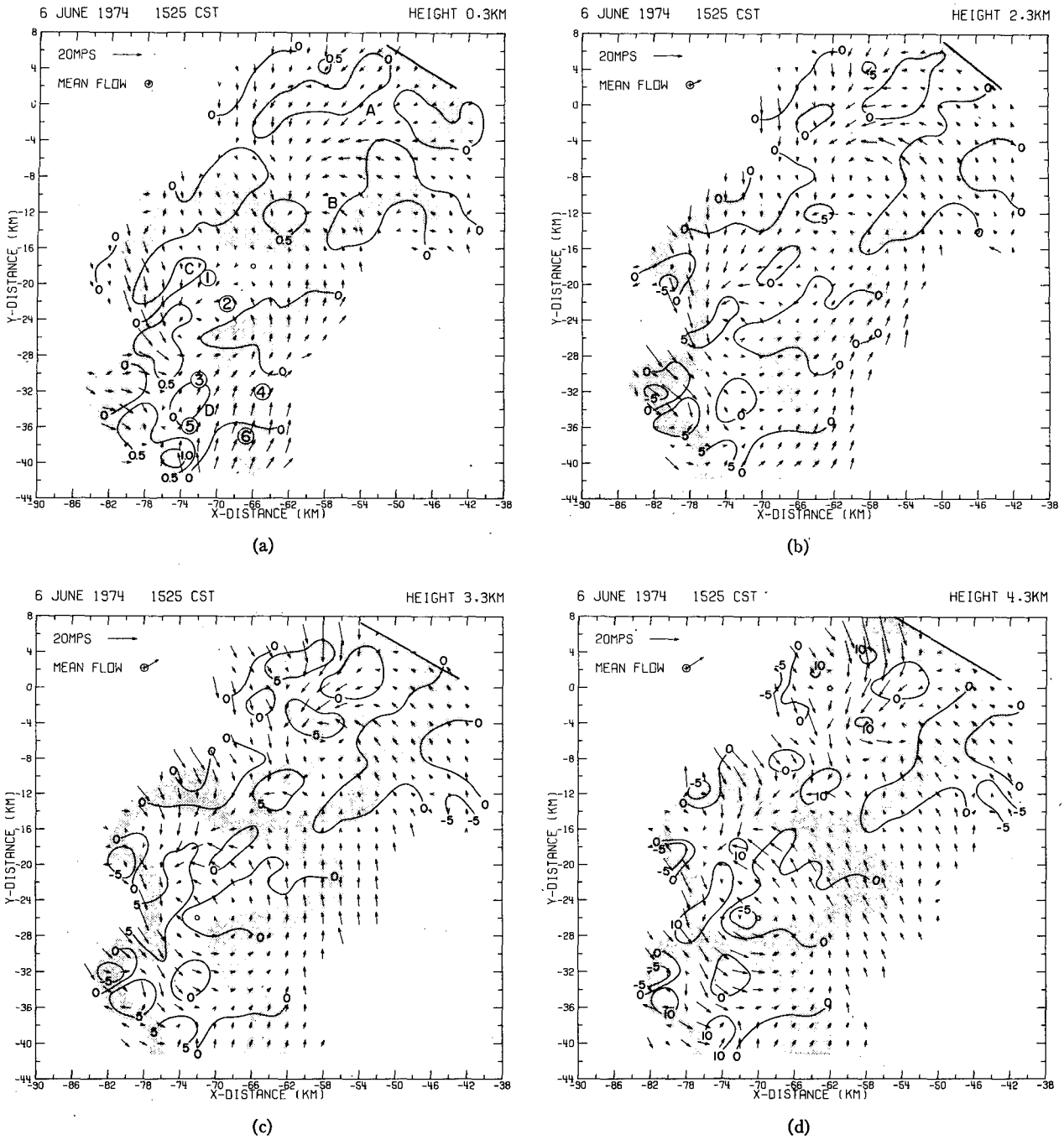

FIG. 3. Horizontal perturbation wind flow and selected contours of vertical velocity (m s^{-1}) for heights above ground of (a) 0.3, (b) 2.3, (c) 3.3 and (d) 4.3 km at 1525 CST. Circles represent horizontal velocities less than 0.5 m s^{-1}. Radar reflectivity (Norman Doppler) between 30 and 40 dBZ shaded. Edge of data collection shown as heavy solid line. Circled numbers refer to hail observations listed in Table 2. North is toward the top of the page.

base (Fig. 4a), and a well-defined gust front (the convergent boundary separating inflow from outflow) extended southward. Single Doppler measurements suggest the updraft mesocyclone actually descended at approximately 1550. An abbreviated sequence of meteorological events recorded at NSSL's Tabler, Okla., mesonet site (see Fig. 4a and Table 3) attests to gust front severity.

Horizontal flow patterns and an east–west vertical section through the cyclone center (Fig. 5) show updraft air entered the storm's right forward flank at low levels and that principal maxima had roots at the

gust front and within the convergent zone west of the mesocyclone. The principal downdraft, both in terms of areal coverage and intensity, was located in the northeastern quadrant of the storm. Middle level air entering the storm ahead of the principal updraft and perhaps descending due to evaporative cooling appears to be the source for this downdraft. However, highest surface wet bulb potential temperatures $\geqslant 20°C$ beneath central portions of the reflectivity core indicates some mixing in heavy rain areas with air originating at low levels. In contrast, lowest wet-bulb potential temperatures on the southwestern (right rear) storm flank ($\leqslant 18°C$) imply little mixing for air descending via a second major downdraft found on the storm's western boundary. Flow from both downdrafts combined near ground to produce the gust front. Dry mid-level

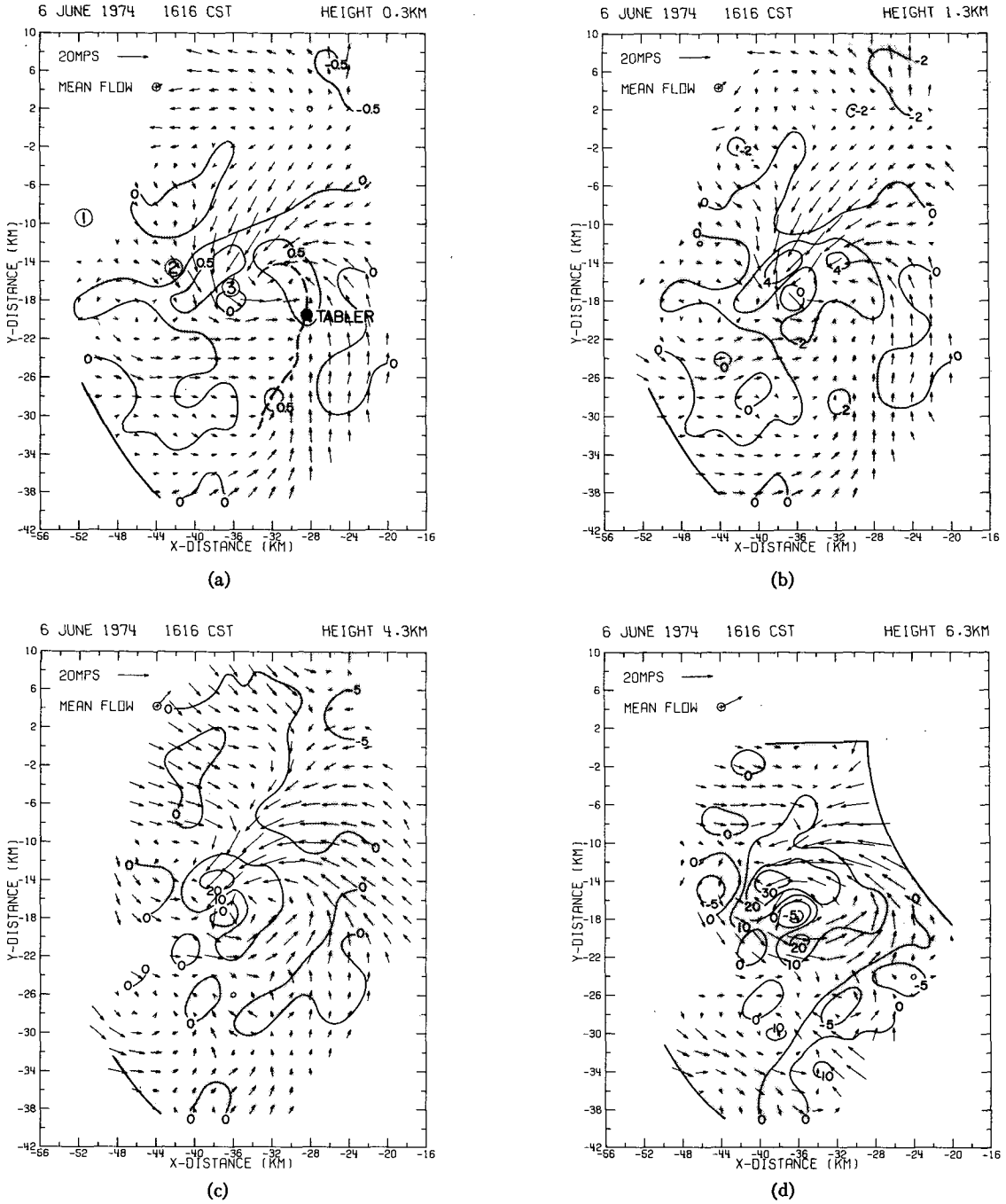

FIG. 4. As in Fig. 3 but for heights above ground of (a) 0.3, (b) 1.3, (c) 4.3 and (d) 6.3 km at 1616 CST. Gust front shown as heavy dashed line.

TABLE 3. Meteorological events recorded at Tabler, Okla., on 6 June 1974. Winds are relative to ground.

1600	Temperature 28°C
1610	Minimum mesoscale pressure recorded
1615	Wind shift from east-southeast to west-northwest
1617	Onset of temperature break
1624	Step increase in wind speed to 23 m s^{-1}, onset of heavy rainfall
1628	Minimum microscale pressure recorded, pressure drop 4 mb. Minimum temperature 18°C
1629	Peak wind gust, west-northwest at 42 m s^{-1}
1632	Pressure rise of 7 mb
1650	Rainfall ends, accumulation 11.2 mm

air entering the storm's eastern and western quadrants did not penetrate the mesocyclone but tended to be diverted by the strong vertical and horizontal flow. Thus, the cores of the updraft and circulation were essentially undiluted by dry environmental air.

Maximum radar echo tops and highest reflectivity measurements aloft were close to the mesocyclone center. Reported hail from storm AB was along the track of the mesocyclone and somewhat smaller than fell from storms C and D (Table 2). Receiver saturation prevented accurate estimates of peak reflectivity values with the Doppler radars. However, measurements with the WSR-57 radar revealed values in excess of 50 dBZ until 1630.

Although not now in evidence, an embedded "hook echo" was observed briefly from 1600 to 1607 (Fig. 6a).

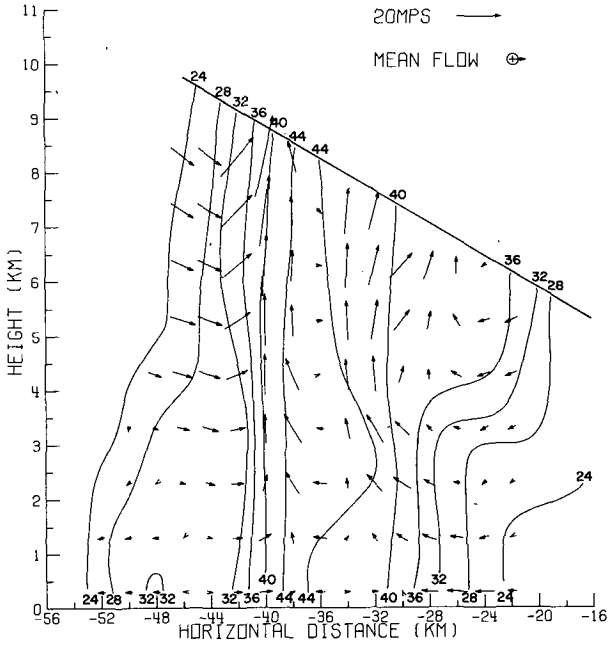

FIG. 5. East–west vertical cross section during mature stage (1616) at $y=-16$ km. The mean u component (6.7 m s^{-1}) has been removed. Note fourfold distortion in vertical axis. Radar reflectivity (Norman Doppler) contoured in dBZ.

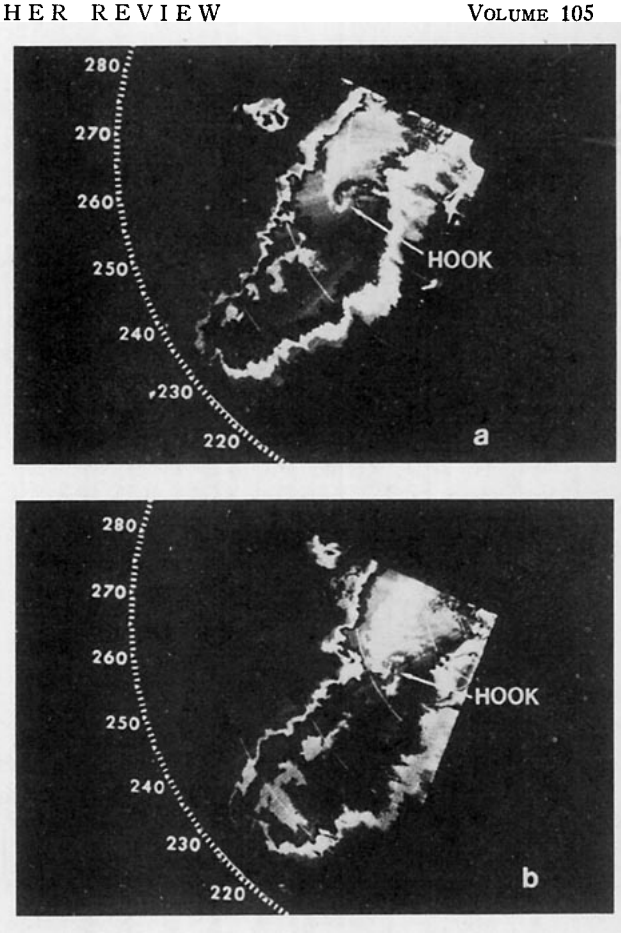

FIG. 6. Contoured PPI display (not range normalized) showing location of intermittent radar hook echo at (a) 1605 and (b) 1624 CST relative to main storm body. Range marks are 20 km.

Single Doppler measurements show that while the hook was in existence, there was also a temporary increase in horizontal flow about the mesocyclone. The hook location (1605), superimposed on the storm total rainfall pattern (Fig. 2), coincides with a distinct maximum >24 mm along the path traversed by the southern storm flank.

c. Onset of storm dissipation: 1625 CST

From 1616 to 1625, downdrafts and low-level horizontal wind speeds increased (Fig. 7) and a small hook echo reformed (Fig. 6b). (Analysis smoothing obliterates the hook feature in Fig. 7a.) Rainfall increased and several precipitation shafts associated with smaller storm cells to the east, observed only aloft earlier, now reached the ground.

Circulation size decreased with height to little more than a shear zone between a distinctive anticyclonic wind feature to the north and a new larger cyclonic circulation to the south (Fig. 7d). In the uppermost portion of the storm only the new circulation near the strongest updrafts could be found.

Eventually heavy precipitation (reflectivities ≥ 40

dBZ) extended from the main storm core to a developing cell 20 km southeast (Fig. 7a). Cutoff of warm moist inflow air and growth of the second updraft (either would reduce latent heat supply) are possible explanations for storm dissipation.

d. Additional storm features

At its most vigorous stage, the surface gust front lengthened to more than 20 km and strong wind surges on scales of several kilometers produced a perturbed wind-shift discontinuity with regions of large speed and directional shears (Fig. 7a). Near the mesocyclone center anomalous shear (6×10^{-2} s^{-1}) on the scale of 1 km was found in the 0° unsmoothed Doppler measurements. Similar persistent high shears, extending through large vertical cloud heights, have been found to correspond with tornadoes in other storms (Burgess *et al.* 1975). Maximum vorticity (1.1×10^{-2}

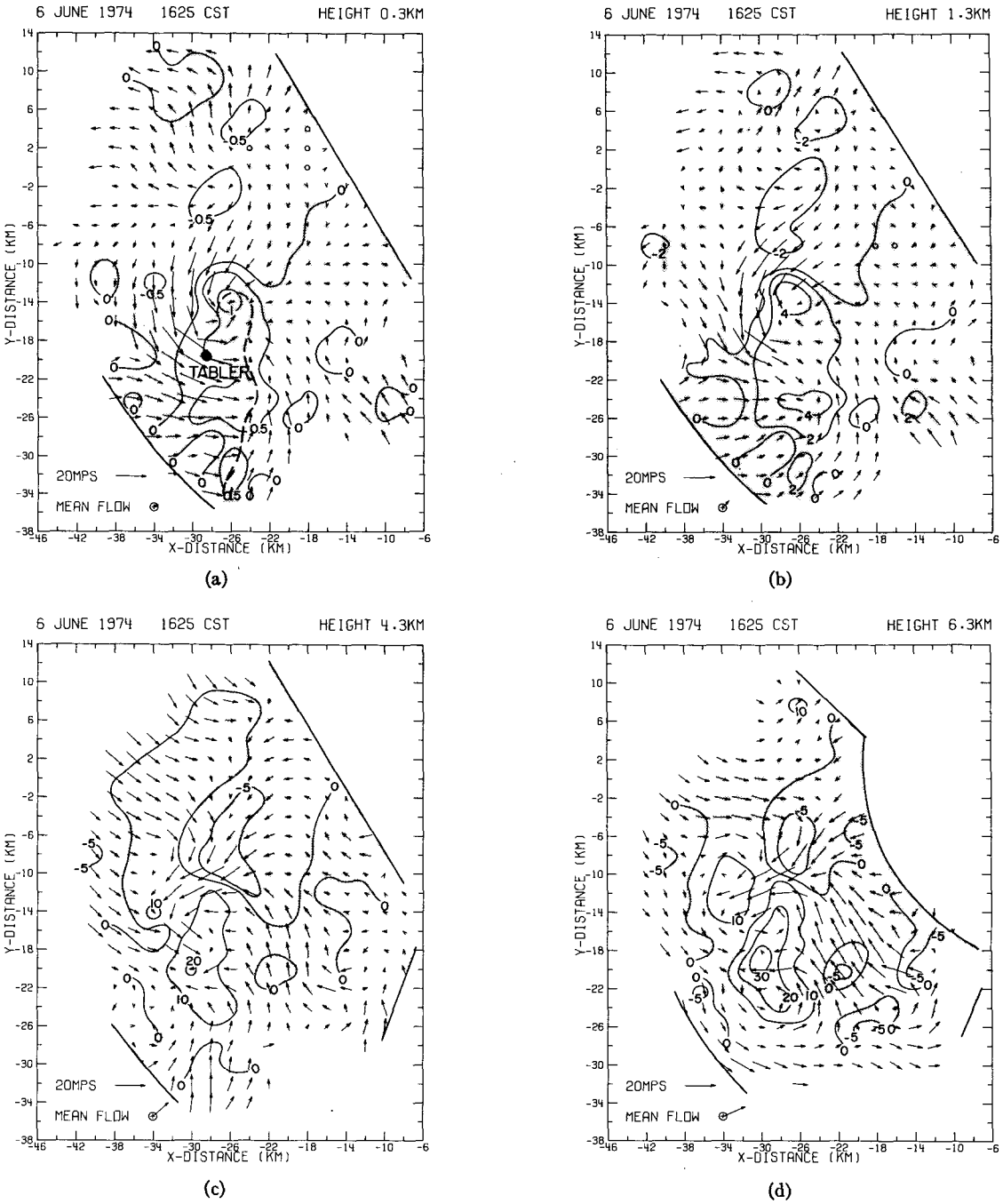

FIG. 7. As in Fig. 4 except at 1625 CST.

s^{-1}, 0.3 km elevation) was at the mesocyclone center and secondary maxima ($\sim 0.3 \times 10^{-2}$ s^{-1}) were located along the gust front. Colocated with the vorticity centers were convergence maxima $\geqslant 0.3 \times 10^{-2}$ s^{-1}. Although a tornado funnel was not reported, the existence of a localized cyclonic shear zone, wind damage and structural similarities with well-documented tornadic storms currently being investigated—all point to an intense tornado-like vortex near ground.

Also of interest is the complexity of AB's rainfall pattern (Fig. 2) with several extrema. Rainfall variability may be related to the high wind velocity spatial variance (Figs. 4 and 7). Note, for example, the rainfall maxima that match the hook echo locations. Apparently, these maxima reflect downdraft intensification and result from precipitation particles swept from the main radar echo body by an accompanying increase in horizontal flow about the mesocyclone. Rainfall was less when the hook was not prominent (i.e., from 1607 to 1620). These data differ slightly from Browning (1964) who found heaviest rainfall beneath left-hand parts of severe right moving storms.

5. Conclusion

Overall Doppler derived wind patterns (mature stage) are similar to the basic severe storm flow structure proposed by Browning (1964), Fankhauser (1971), and others. Low-level moist and potentially warm air approaches the storm from the right forward flank, curves cyclonically, and as deduced by Browning may back significantly before exiting in the anvil. Source air for the major downdraft residing on the forward left flank enters the storm's forward flanks at middle levels and passes ahead of the updraft. A departure in the 6 June storm from proposed models appears to be a second persistent downdraft on the western edge of the storm. Both downdrafts may have been initiated by evaporative cooling.

Synthesis of wind flow and raingage observations (i.e., temporary increases in low-level horizontal wind speed, rainfall deposition, plus the downdraft intensification found at 1625) support the tentative conclusion that hook echo development reflects downdraft intensification (pulsation) and ensuing horizontal acceleration of droplet-laden air. Interaction between outflow and inflow appears to yield the characteristic hook shape.

In all, six cyclonic circulations were found in the single and dual-Doppler measurements collected on 6 June 1974. Thus, this property may be fairly common with intense storms. Two circulations were observed only at mid-levels (4–6 km) and four extended from ground level to large vertical heights. Examination of three storms which produced reported damaging surface winds suggest the following characteristics of updraft mesocyclone evolution. Cyclonic rotation first occurs aloft and the level of detectable circulation lowers with time. Descent presumedly coincides with a local increase in the three-dimensional wind flow and when damaging surface winds occur, an intense mesocyclonic circulation is present at ground levels. Dissipation is defined by diminishing updrafts and decreased horizontal wind speeds aloft. The mechanism whereby rotation is initiated and factors that determine the subsequent development and lowering of the concentrated circulation await further investigation.

Acknowledgments. The author is indebted to NSSL staff who assisted in the preparation of this report. I am particularly grateful to Drs. Ron Alberty, Joseph Schaefer, and Peter Ray and Mr. Rodger Brown for their critical reviews and discussions. Messrs. Rodger Brown and Charles Safford were principals in the formulation of the dual-Doppler analysis scheme. Mrs. Connie Hall typed the various drafts of the manuscript. The hail observations were provided by Mr. Stephan Nelson and the dense raingage observations were made available by the Agriculture Research Service (ARS), U. S. Department of Agriculture, Chichasha, Okla.

REFERENCES

Armijo, L., 1969: A theory for the determination of wind and precipitation velocities with Doppler radars. *J. Atmos. Sci.*, **26**, 570–573.

Barnes, S. L., 1964: A technique for maximizing details in numerical weather map analysis. *J. Appl. Meteor.*, **3**, 396–409.

Brandes, E. A., 1975: Optimizing rainfall estimates with the aid of radar. *J. Appl. Meteor.*, **14**, 1339–1345.

Browning, K. A., 1964: Airflow and precipitation trajectories within severe local storms which travel to the right of the winds. *J. Atmos. Sci.*, **21**, 634–639.

Burgess, D. W., L. R. Lemon and R. A. Brown, 1975: Tornado characteristics revealed by Doppler radar. *Geophys. Res. Lett.*, **2**, 183–184.

Dennis, A. S., C. A. Schock and A. Koscielski, 1970: Characteristics of hailstorms of western South Dakota. *J. Appl. Meteor.*, **9**, 127–135.

Fankhauser, J. C., 1971: Thunderstorm-environment interactions determined from aircraft and radar observations. *Mon. Wea. Rev.*, **99**, 171–192.

Foote, G. B., and P. S. du Toit, 1969: Terminal velocity of raindrops aloft. *J. Appl. Meteor.*, **8**, 249–253.

Kropfli, R. A., and L. J. Miller, 1976: Kinematic structure and flux quantities in a convective storm from dual-Doppler radar observations. *J. Atmos. Sci.*, **33**, 520–529.

Lhermitte, R. M., and M. Gilet, 1975: Dual-Doppler radar observation and study of sea breeze convective storm development. *J. Appl. Meteor.*, **14**, 1346–1361.

Marwitz, J. D., 1972: The structure and motion of severe hailstorms. Part 1: Supercell storms. *J. Appl. Meteor.*, **11**, 166–179.

Ogura, Y., and N. A. Phillips, 1962: Scale analysis of deep and shallow convection in the atmosphere. *J. Atmos. Sci.*, **19**, 173–179.

Ray, P. S., R. J. Doviak, G. B. Walker, D. Sirmans, J. Carter, and B. Bumgarner, 1975: Dual-Doppler observation of a tornadic storm. *J. Appl. Meteor.*, **14**, 1521–1530.

Rogers, R. R., 1964: An extension of the Z-R relation for Doppler radar. *Preprints 11th Weather Radar Conf.*, Boulder, Colo., Amer. Meteor. Soc., 158–161.

Sirmans, D., and B. Bumgarner, 1975: Numerical comparison of five mean frequency estimators. *J. Appl. Meteor.*, **14**, 991–1003.